NUMERICAL ANALYSIS ON THE THERMAL PERFORMANCES OF DIFFERENT TYPES OF FIN HEAT SINK FOR HIGH-POWER LED LAMP COOLING

Yicang HUANG [1], Shengnan SHEN [1], Hui LI [1,*], and Yunjie GU [1]

[1] Research Center of Electronic Manufacturing and Packaging Integration, School of Power and Mechanical Engineering, Wuhan University, Wuhan 430072, China

[*] Corresponding author; E-mail: li_hui@whu.edu.cn

The efficient cooling is very important for a light emitting diode (LED) module because both the energy efficiency and lifespan decrease significantly as the junction temperature increases. Fin heat sinks are commonly used for cooling LED modules under natural convection conditions. This work proposed two novel models of fin heat sink, named the pin-plate fin heat sink (PPF) and the oblique-plate fin heat sink (OPF), by combining plate fins with pin fins and oblique fins and their thermal performances were studied numerically. The LED module was assumed to be operated under 1 atmospheric pressure and its heat input is set to 4 watts. The PPF with 8 plate fins inside (PPF-8) and the OPF with 7 plate fins inside (OPF-7) show the best thermal performances among all PPF and OPF designs. Total thermal resistances of PPF-8 and OPF-7 decreased by 9.0% - 15.6% compared to those of three original models. And heat transfer coefficients of PPF-8 and OPF-7 were higher by 12.6% - 35.2% than those of three original heat sinks.

Key words*: light emitting diode (LED), fin heat sink, thermal design, natural convection*

1. Introduction

Nowadays, light emitting diodes (LEDs) play an important role in the illumination market. LEDs are widely used in varieties of applications as diverse as indoor/outdoor lights, aviation lighting, backlight units for display devices, automotive headlamps, and fishery lights [1]. In an LED module, about 20% of electric power is used for light emitting, while the rest is converted into heat [2]. With the increase of input power, the junction temperature of an LED module can drastically rise to a high level [3]. A high junction temperature results in reductions of the energy efficiency, light intensity, and lifespan [4]. Therefore, an efficient cooling device is very important for an LED module to dissipate the heat generated by the chip into ambient air.

Cooling technologies for the LED module can be divided into active and passive methods [5]. Passive methods dissipate the heat with natural convection conditions while active methods use the forced convection. Passive cooling methods are preferred for LED devices because these methods get a high reliability due to that they do not require additional moving parts [5, 6]. The fin heat sink as a passive cooling method is commonly used for cooling LED modules with natural convection conditions due to its easy implementation, low operation cost, and high reliability.

In 1942, Elenbass [7] explored the thermal performance of parallel plates under natural convection conditions. Then, Bodoia and Osterle [8] numerically studied the flow and heat-transfer characteristics of the vertical plates and achieved a good agreement with the data of Elenbass except for low values of Grashoff number. Starner and McManus [9] experimentally investigated the orientation effect on the heat transfer coefficients for fin arrays. It was found that the vertical arrays presented 10 to 30 percent below on the heat transfer coefficients than those of horizontal arrays and the coefficients of 45-degree arrays were 5 to 20 percent below those of the vertical arrays. Welling and Wooldridge [10] presented an experimental study on parameters of fin height and fin width. The results suggested that there was an optimum fin height for each fin channel width. Cha and Cha [11] investigated laminar steady buoyancy-driven flow around two interacting cubes in a finite medium by employing a control-volume finite difference technique. The numerical results were in good agreement with the holographic interferograms. Rammohan and Venkateshan [12] presented an interferometric study on heat transfer by natural convection and radiation in a horizontal array. It was concluded that there was a mutual interaction between natural convection and radiation which indicated that a simplistic approach based on the simple superposition of radiation and convection heat transfer calculated independently was unsatisfactory. Lee et al. [13] employed sectional oblique fins in a micro-channel heat sink and enhanced thermal performance of the fin heat sink which was attributed to the better fluid mixing and the reinitialization of the thermal boundary layer at the leading edge of each oblique fin. Many other studies [14–24] concerned more about the geometric parameters of plate fin arrays. And similarly to Staner and McManus [9], some researchers [5, 25–28] analyzed the orientation effect of plate fin arrays under natural convection conditions.

For LED lighting applications, lots of studies have been done in recent years to improve the thermal performance of fin heat sinks used for high-power LED lamp. Christensen and Graham [6] numerically studied the package and system level temperature distributions of a high-power LED array and suggested that attention must be focused on providing the highest convective heat transfer coefficients while improving the packaging design of LED applications. Jang et al. [29, 30] optimized the cooling performance and mass of a pin-fin radial heat sink and succeed in reducing the mass of heat sink by more than 30% while maintaining a similar cooling performance to that of a plate-fin heat sink studied in a previous study. Similarly, Yu et al. [31] performed parametric studies on optimizing a radial heat sink under natural convection conditions. They compared the effects of the number of fins, fin length and heat flux on the thermal resistance and average heat transfer coefficient. Ha and Graham [4] conducted a thermal analysis of high-power LED packages implementing chip-on-board (COB) architecture combined with power electronic substrate. Cheng et al. [2] presented an integrated multi-fin heat sink design with a fan on metal core printed circuit board (MCPCB) substrate for a high-power LED array. The results of this work suggested that a back lighting panel with a fan can increase the lifespan of LED module. Huang et al. [32] introduced perforations through the fin base for long horizontal rectangular fin arrays and achieved a significantly improved heat transfer performance. Based on Huang's work, Jeong et al. [1] employed the perforations both in fin base and fins to improve air circulation. And many other studies [3, 33, 34] have also been carried out to improve thermal performance of fin heat sinks for high-power LED lamp cooling by various methods.

This work proposed a new design method for the high-power LED lamp cooling with natural convection conditions by combining plate fins with pin fins and oblique fins. Two novel models of fin heat sink called the pin-plate fin heat sink (PPF) and the oblique-plate fin heat sink (OPF) were

designed and their heat dissipation performances were compared with those of three original fin heat sinks. Furthermore, a parametric study on the number of plate fins in PPF and OPF are conducted to find the optimized model.

2. Numerical method

2.1. Physical model

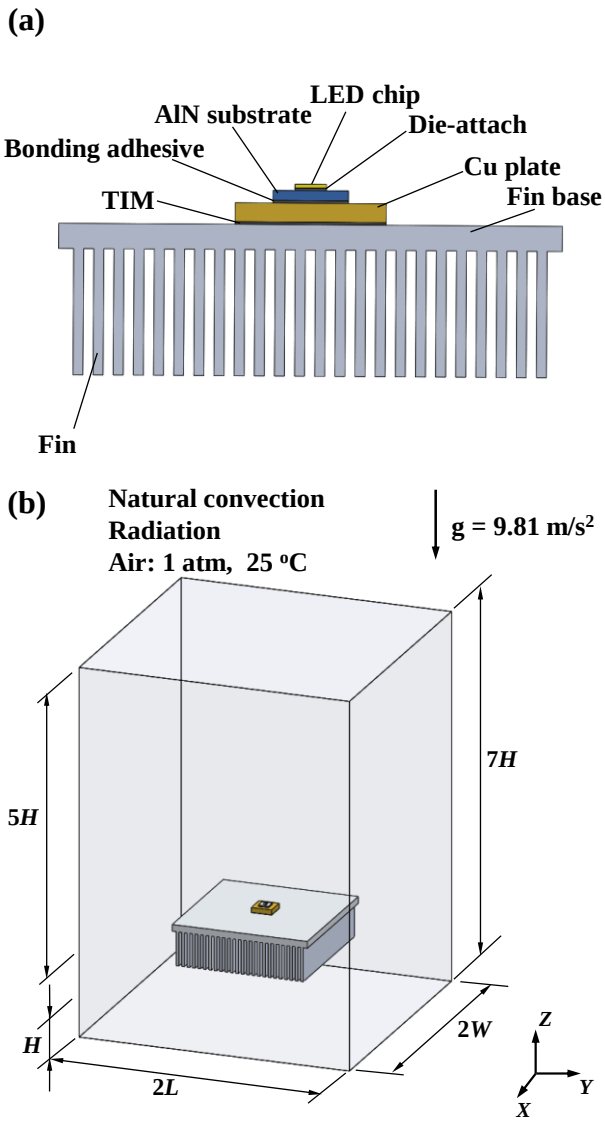

Fig. 1. (a) LED module on the fin heat sink, and (b) computational domain.

This study is set up as a three-dimensional fluid-solid conjugate problem to investigate the thermal performances of 5 models of fin heat sink used for high-power LED lamp cooling. The structural schematic of an LED module and the computational model is illustrated in Fig. 1. As show in Fig. 1(a), the LED module is mounted on a fin heat sink, and consists of an LED chip, an aluminum nitride (AlN) substrate, and a copper (Cu) plate below. The fin heat sink is composed of a fin base and number of fins. Additionally, die-attaches and bonding adhesives are used to attach the LED chip and AlN substrate, respectively. And the thermal interface material (TIM) is used to bond the LED module to the fin heat sink. Table 1 shows geometric specifications of the LED module. Fig. 1(b) shows the

computational domain and operating conditions. The scale of the computational domain is determined by taking both heat transfer characteristics and computational time into consideration [5, 31]. The height of the domain above the LED module is chosen as 5*H* while the domain below is *H*, where *H* represents the total height of the LED module with fin heat sink. The width and length of the domain is 2*W* and 2*L*, where *W* and *L* represent the width and length of the fin heat sink, respectively. The model works under natural convection conditions and the pressure of ambient air is set to be 1 atmospheric pressure (atm) and the air temperature is 25 °C. The radiation heat transfer and gravitational acceleration (*g*) are taken into consideration in this study. The *g* is assumed to be 9.81 m/s^2 along the opposite of *Z*-direction.

Table 1. Geometric specifications of the LED module

Component	Wdith × Length (mm)	Thickness (mm)
LED chip	1.0 × 1.0	0.10
Die-attach	1.0 × 1.0	0.02
AlN substrate	3.0 × 3.0	0.38
Bonding adhesive	3.0 × 3.0	0.02
Cu plate	6.0 × 6.0	1.5
TIM	6.0 × 6.0	0.02

The heat sink consists of a fin base with a thickness of 2 mm and numbers of fins with a height of 10 mm. Fig. 2 presents specific dimensions of fin heat sinks. The pin fin used in all models has a length of 2.4 mm, a width of 0.8 mm, and a height of 10 mm. Similarly, the oblique fin has a length of 2.4 mm, a width of 0.8 mm, and a height of 10 mm. The cross section of oblique fin is a parallelogram with an acute angle of 27^o [13].

2.2. Numerical methods

The natural convection is governed by the Prandtl number and the Rayleigh number:

$$\mathrm{Pr} = \nu / \alpha \tag{1}$$

$$\mathrm{Ra} = \frac{g\beta\Delta T L_r^{\,3}}{\nu^2}\mathrm{Pr} \tag{2}$$

where all properties refer to the air involving the heat sink. Then, the Rayleigh number, Ra ≈ 2 × 10^6, is well below the typical transition value of 10^8 - 10^9 for the turbulent regime [34]. Therefore, the flow field exhibits a laminar flow. Other assumptions made to simplify the analysis are as follows [35]:

(1) The air is assumed to be steady and incompressible.

(2) The thermophysical properties of air and solids are constant.

(3) All surfaces are gray and diffuse.

The commercial CFD software, ANSYS Fluent 15.0, is used for solving the continuity, momentum and thermal energy equations for air and solids. The radiation heat transfer rate is solved by the discrete ordinates method [36]. The external boundaries of the computation domain are set as pressure-outlets. The cell zone of the LED chip is set as the heat source of which the energy is 80% of the input power of the LED lamp [2]. The conjugated heat transfer is considered at the interface of the fluid and solid domains [36]. Thermophysical properties of materials are presented in Table 2 [37].

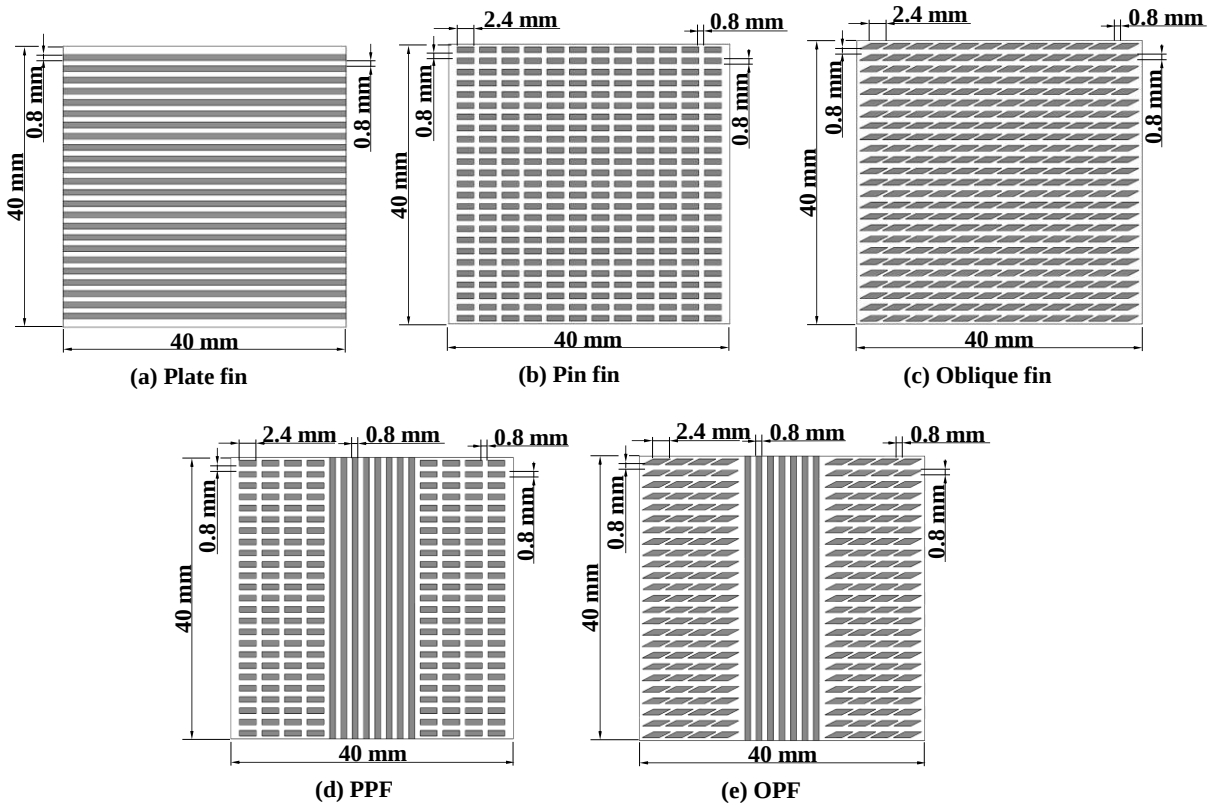

Fig. 2. Specifications of original and proposed fin heat sinks.

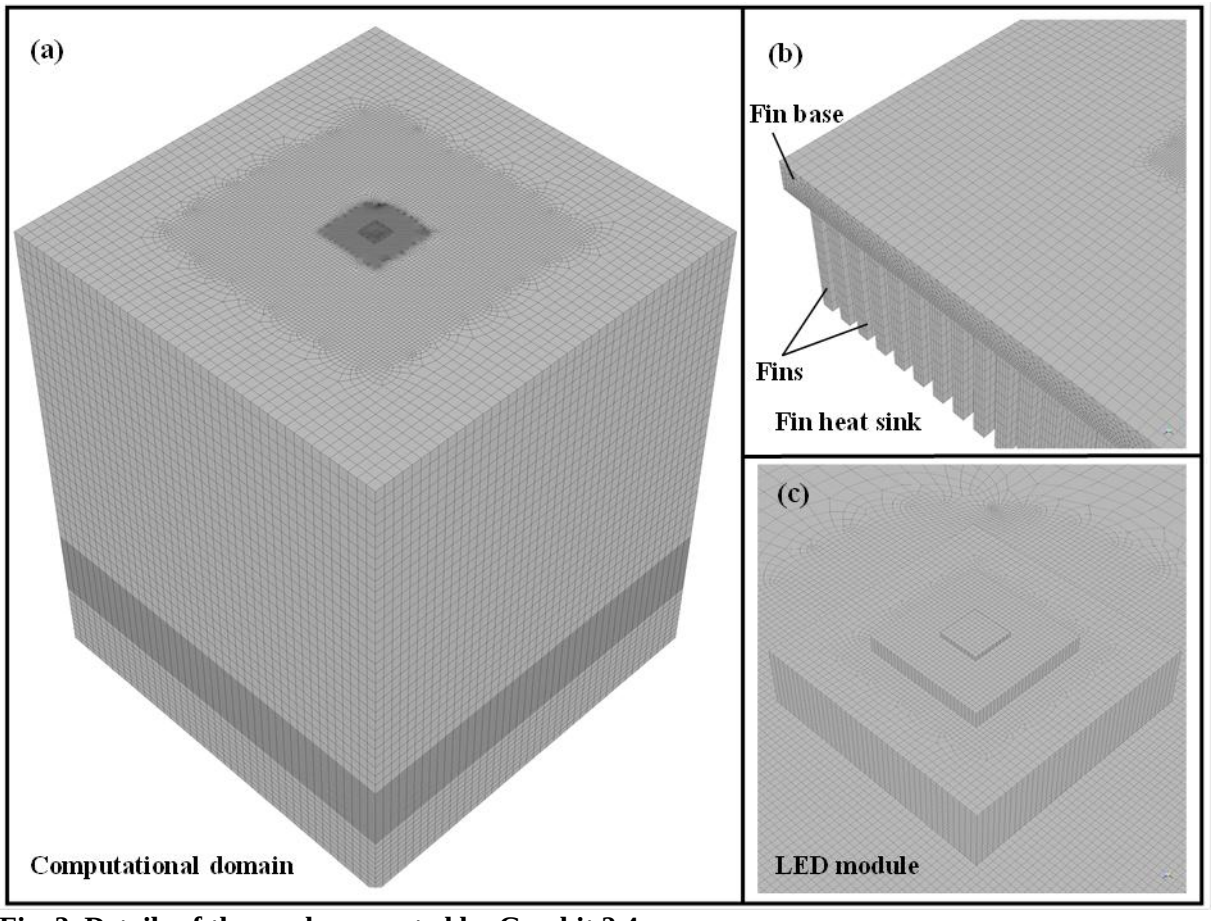

Fig. 3. Details of the mesh generated by Gambit 2.4.

Table 2. Thermophysical properties of materials

Materials	ρ (kg/m^3)	c_p (J/kg K)	k (W/m K)	ε
LED chip	6070	490	130	0.9
Die-attach	14510	710	57	0.9
AlN substrate	3235	760	150	0.9
Cu plate	8978	381	387.6	0.78
TIM	2260	1700	3.5	0.9
Fin heat sink	2719	871	202.4	0.55

Nonuniform mesh employed for all cases in this study is generated by Gambit 2.4. The details of the finite element mesh are shown in Fig. 3. For improving accuracy and saving computational time, the size of the mesh for LED module is much smaller than that of the fin heat sink and fluid domain. The semi-implicit method for pressure-linked equations (SIMPLE) algorithm is used to couple the velocity and pressure, and the least squares cell based method is applied for the gradient equation. The body-force-weighted method is applied for the pressure equation, and the second-order-upwind method is used to discretize the momentum, energy, and discrete ordinates equations.

2.3. Data reduction

The heat transfer coefficient of fin heat sink is calculated by the following equation:

$$\bar{h} = \frac{P_h}{A(\overline{T_s} - T_a)} \tag{3}$$

where P_h is the heat input, which is 80% of the total input electric power of the LED module. In this study, P_h is set to 4 watts because the total input power of LED is 5 watts. A represents the surface area of the fin heat sink. $\overline{T_s}$ represents the average surface temperature of the fin heat sink, and T_a is the ambient air temperature which is 25 °C in this study.

The thermal resistance is one of the most important indicators reflecting thermal performance of an LED cooling device. The total thermal resistance from the LED chip to the ambient air can be expressed as:

$$R_t = \frac{T_j - T_a}{P_h} \tag{4}$$

where T_j represents the junction temperature of the LED chip. Additionally, the masses of different fin heat sinks are evaluated and compared for the purpose of finding out the model with an excellent thermal performance simultaneously with a relative small mass.

2.4. Model validation

The numerical model was then validated by comparing the simulation results with the experimental data presented by Shen et al. [5] using the same geometric structure and operating conditions. As shown in Fig. 4, our simulation results are in good agreement with their experimental results for the number of plate fins (n) of 7 and 11, respectively, and the maximum deviation of junction temperature was only 4.7%. Therefore, our numerical models are effective and reasonable for predicting the thermal performance of heat sink used for high-power LED lamp cooling.

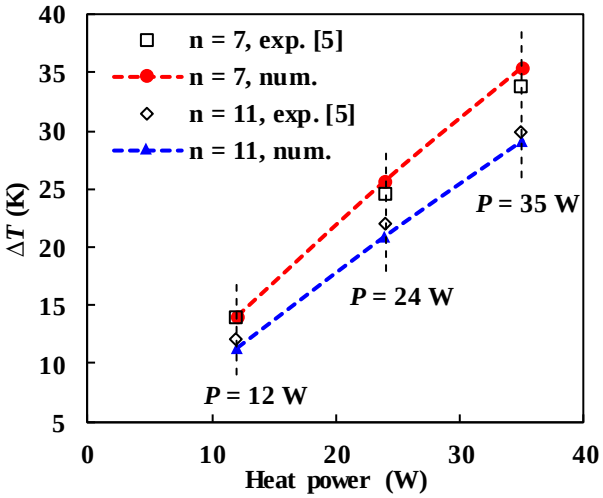

Fig. 4. Validation of the numerical methods used in our work.

Moreover, a grid independency test on the plate fin model was conducted with five different grid numbers. The effects caused by grid numbers on the junction temperature are shown in Fig. 5. The junction temperature makes no considerable difference from the grid number of 2,125,889 to 2,933,860. Therefore, the model with the grid number of 2,125,889 was selected for following simulations by considering both the accuracy and the computational time.

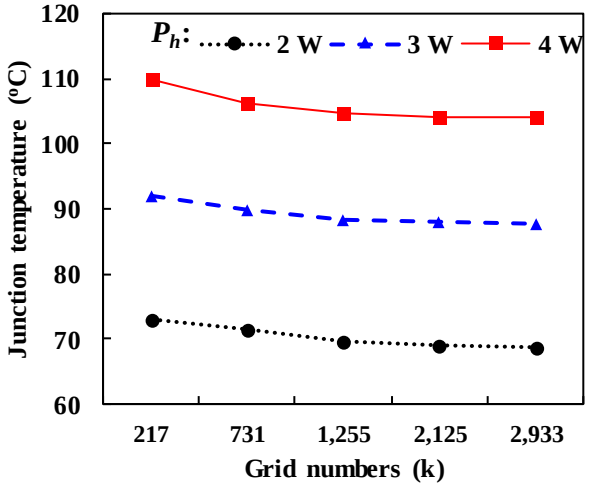

Fig. 5. Grid independency test on the plate fin model for different power of heat input.

3. Results and discussions

3.1. Comparison of the proposed models and original models in terms of heat dissipation performance

All cooling models studied in this work are assumed to be operated under same conditions of which the operating pressure is 1 atm and the ambient air temperature is 25 °C. Heat inputs of all models are set to 4 watts. Fig. 6 shows temperature contours of different models. The plane which is parallel to the *X*-*Z* plane locates in the centre of the computational domain. Junction temperatures are labelled in each contour. Fig. 6(a), (b), and (c) show temperature contours of three original models while (d) and (e) exhibit contours of two proposed models. The highest temperature appears at the LED chip because the chip is the heat source. The heat firstly transfers from the LED chip to the cold

Cu plate and then to the fin heat sink by heat conduction, and the heat is finally dissipated into the ambient air. Then, there is an obvious drop of temperature exhibited in Fig. 6 from the chip, through the AlN substrate and Cu plate, to the fin heat sink. Moreover, the junction temperatures of proposed models are lower by 6 ℃ – 12 ℃ than those of three original models. It indicates that the proposed models have a better heat dissipation performance than three original models.

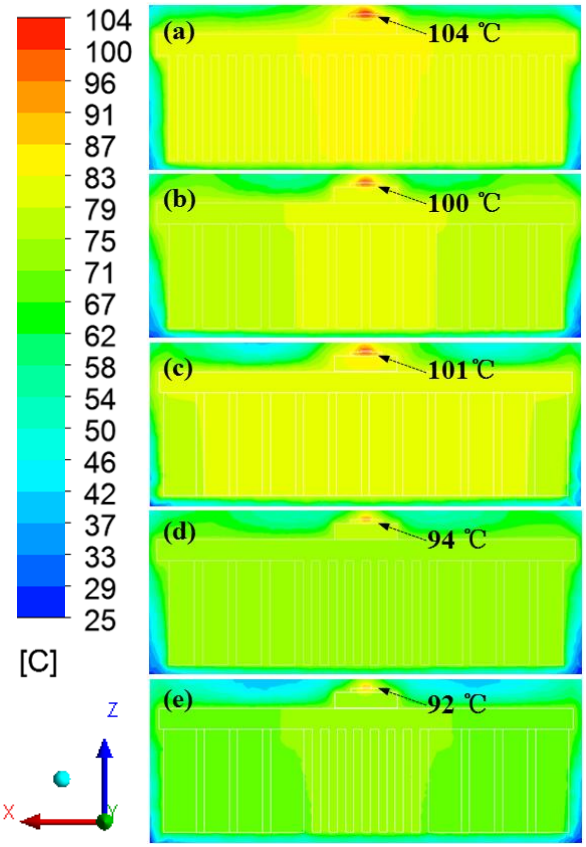

Fig. 6. Temperature contours of (a) plate fin, (b) pin fin, (c) oblique fin, (d) PPF, and (e) OPF model.

Figure 7 compares the detailed temperature distribution along *X* and *Y* directions on the top surface of fin heat sinks. The plate fin heat sink shown in Fig. 7(a) has a much lower temperature gradient along the *Y*-direction than that along the *X*-direction which means the plate fin heat sink has a higher heat dissipation performance along the *Y*-direction due to the continuity of solids along this direction. In contrast, the pin fin and oblique fin heat sink, shown in Fig. 7(b) and (c), exhibit a bit higher temperature gradient along the *Y*-direction because the length of the fin along the *X*-direction is three times larger than that along the *Y*-direction. However, due to the large surface area and many small gaps created among fins, maximum temperatures of the pin fin and oblique fin model are lower by 5 °C and 3 °C than that of the plate fin model, respectively. Proposed models shown in Fig. 7(d) and (e) combine thermal advantages of the plate fin with the pin fin and oblique fin. Plate fins mounted in the centre of the PPF and OPF heat sink strengthen the heat dissipation performance along the *Y*-direction. Pin fins and oblique fins in the PPF and OPF heat sink increase the total surface area and bring lots of small gaps which benefit to the flowing and mixing of the air. As a result, the temperature distributed on the top surface of the PPF and OPF heat sinks are much lower than those of three original heat sinks. And the different heat dissipation performances along different directions are

also obviously illustrated in Fig. 8 which shows the temperature distribution on heat sinks from the bottom view. As shown in Fig. 8(a), (d) and (e), plate fins in the heat sink easily take heat from the center to the edge along the *Y*-direction. However, the pin fins and oblique fins shown in Fig. 8(b) and (c) slightly strengthen the heat dissipation performance along the *X*-direction.

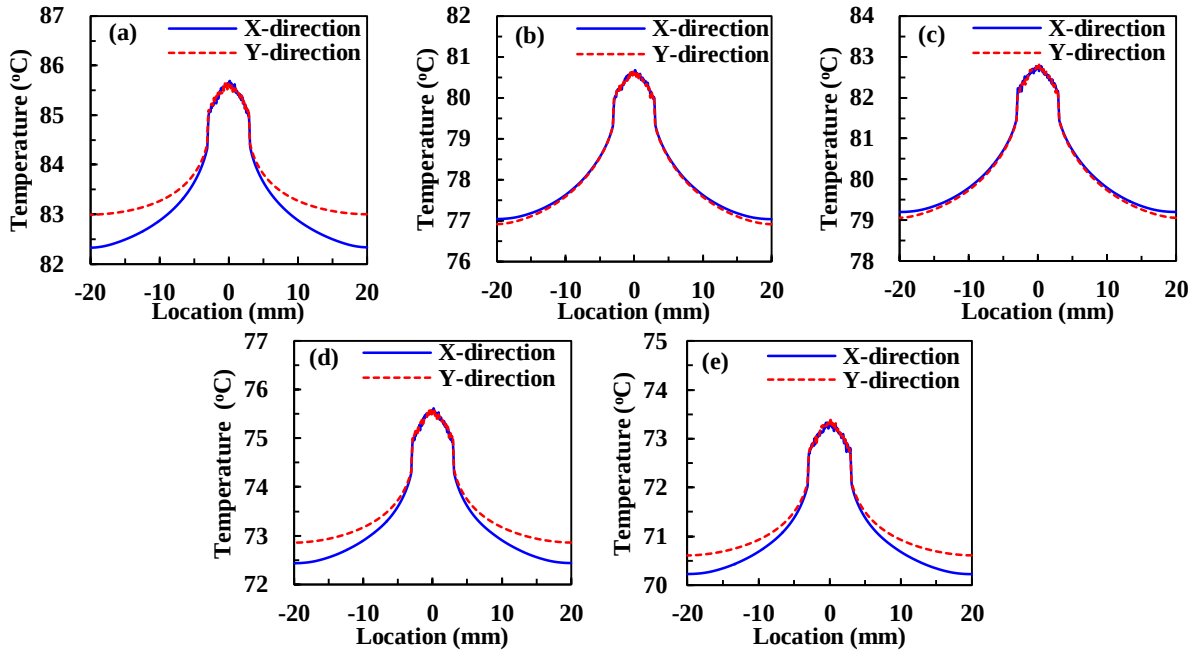

Fig. 7. Temperature profiles along *X* and *Y* directions on the top surface of (a) plate fin, (b) pin fin, (c) oblique fin, (d) PPF, and (e) OPF heat sink.

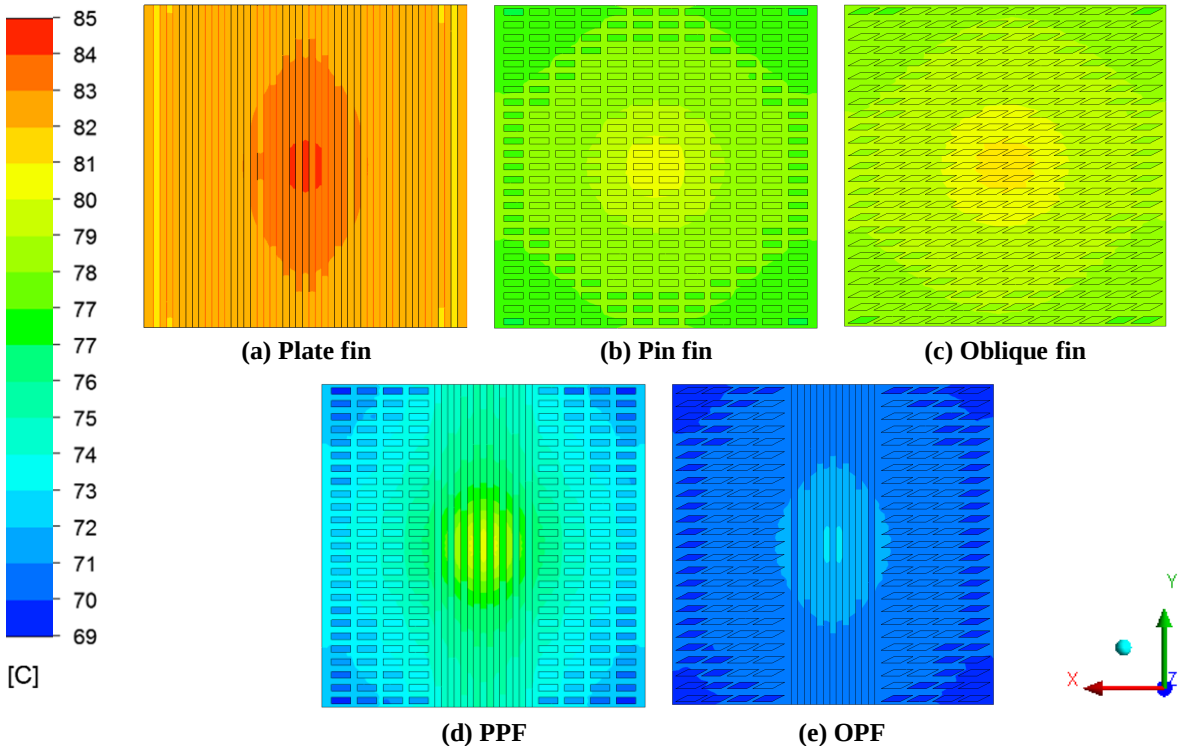

Fig. 8. Temperature distribution of original and proposed models from the bottom view.

3.2. Optimization of proposed models

Then, we studied forward to the further optimization of proposed models by varying the number of plate fins mounted in the PPF and OPF heat sink. The number of plate fins in each PPF heat sink (N_1) is varying as 0, 4, 8, 12, 16, 20, and 24. The number of the plate fins in each OPF model (N_2) is varying as 0, 3, 7, 11, 15, 19, and 24. Differences between N_1 and N_2 are caused by the specific geometric dimensions of the pin fins and oblique fins mounted in PPF and OPF models. All PPF and OPF models work under same conditions with the ambient air temperature of 25 °C, operating pressure of 1 atm and heat input of 4 watts.

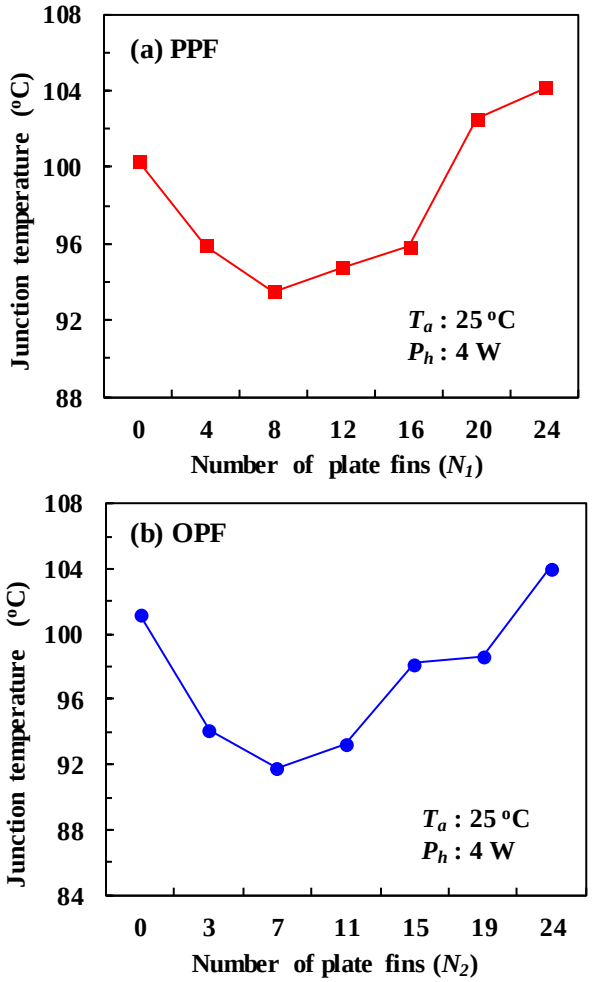

Fig. 9. Variations of junction temperatures of PPF and OPF models with various number of plate fins.

Figure 9 shows variations of the junction temperatures of proposed models with various number of plate fins. Whether in the PPF or OPF models, the junction temperature decreases first and then increases with the increasing of the number of plate fins. As shown in Fig. 9(a), the junction temperature of the PPF model with 8 plate fins (PPF-8) is the lowest among all PPF models. And it is lower by 6.8 °C and 10.6 °C than that of the PPF model with none plate fin (PPF-0) and with 24 plate fins (PPF-24), respectively. Fig. 9(b) shows that the junction temperature of the OPF model with 7 plate fins (OPF-7) is lower than any other OPF models with different plate fins. It is lower than that of the OPF model with none plate fin (OPF-0) and with 24 plate fins (OPF-24) by 9.4 °C and 12.2 °C,

respectively. And the junction temperatures of the PPF-8 and OPF-7 model are 96 °C and 94 °C, respectively, which are well below the critical temperature of 110 °C for the LED module [33].

Figure 10 compares the heat transfer coefficients of PPF and OPF heat sinks with varying number of plate fins. As shown in Eq. (3), the heat transfer coefficient of the fin heat sink is controlled by the surface area, the average surface temperature, and the ambient air temperature. Heat transfer coefficients of PPF and OPF heat sinks increase first and then decrease as the number of the plate fins varying from 0 to 24. As shown in Fig. 10(a), PPF-8 shows a higher heat transfer coefficient than any other PPF heat sinks with different number of plate fins. The heat transfer coefficient of PPF-8 is higher than that of PPF-0 and PPF-24 by 12.5% and 23.8%, respectively. Fig. 10(b) shows that the heat transfer coefficient of OPF-7 is the highest among all OPF heat sinks. And the heat transfer coefficient of OPF-7 is higher by 35.0% and 16.4% than those of OPF-0 and OPF-24, respectively.

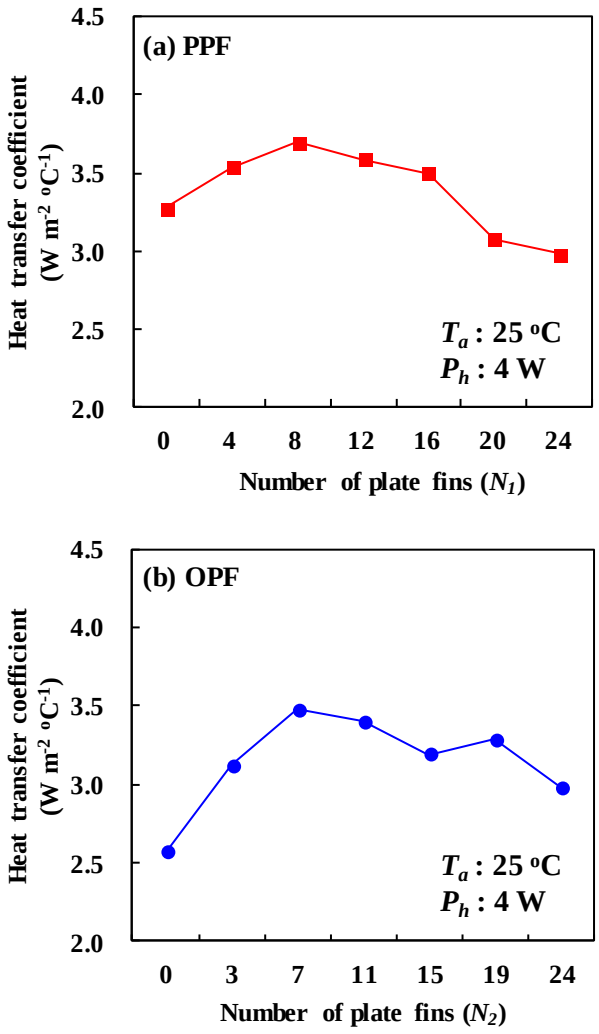

Fig. 10. Variations of the heat transfer coefficients of PPF and OPF models with various number of plate fins.

Figure 11 shows comparisons of the surface area, mass, and total thermal resistance of different PPF and OPF heat sinks. With the increasing of the number of plate fins in the PPF and OPF heat sinks, the surface area decreases while the mass increases, but the total thermal resistance decreases

first and then increases. As shown in Fig. 11(a) and (b), PPF-8 and OPF-7 show the lowest thermal resistance among all PPF and OPF models, respectively. The thermal resistance of PPF-8 is lower by 9.0% and 13.4% than those of PPF-0 and PPF-24, respectively. Similarly, the thermal resistance of OPF-7 is lower than those of OPF-0 and OPF-24 by 12.3% and 15.6%, respectively. It is concluded that PPF-8 and OPF-7 achieve the best thermal performance with a relatively small mass of the material.

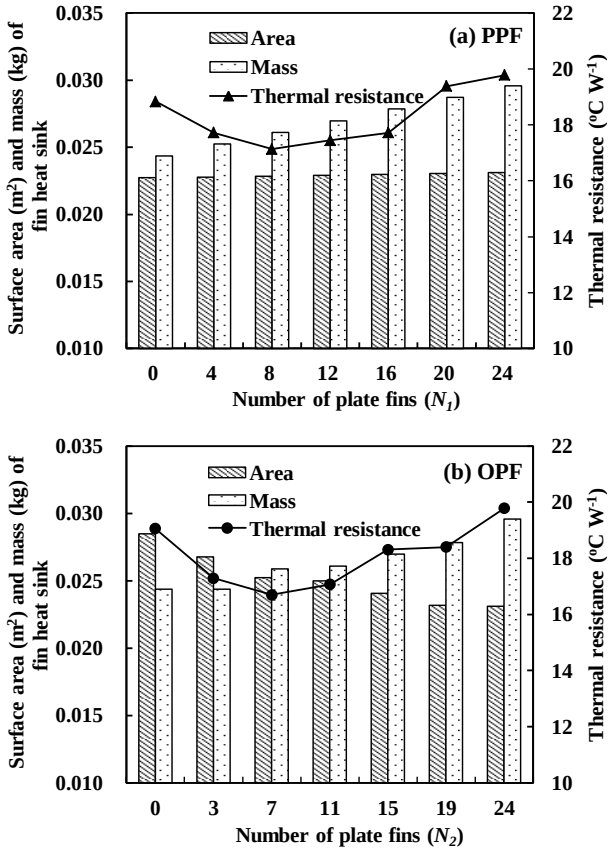

Fig. 11. Variations of the surface area, total mass, and total thermal resistance of PPF and OPF models with various number of plate fins.

4. Conclusions

Novel designs of fin heat sink for high-power LED lamp were proposed and followed to find the most optimized models under natural convection conditions. These two novel models, named the PPF and OPF, were designed by combining plate fins with pin fins and oblique fins, respectively. Novel PPF and OPF models show lower junction temperatures by about 6 °C – 12 °C than those of three original models mainly because the pin fins and oblique fins in the proposed models increase the total surface area and bring lots of small gaps which benefit to the flowing and mixing of the air, and the plate fins mounted in the centre of these models strengthen the heat dissipation performance along the *Y*-direction. Then, the optimizing of novel models was conducted by varying the number of plate fins in PPF and OPF models. And PPF-8 and OPF-7 show the lowest junction temperature and lowest total thermal resistance among all PPF and OPF models, respectively. Junction temperatures of PPF-8 and OPF-7 are lower than those of three original models by about 6 °C – 12 °C. The total thermal

resistances of PPF-8 and OPF-7 show 9.0% – 15.6% smaller than those of original models. And heat transfer coefficients of PPF-8 and OPF-7 are higher by 12.6% – 35.2% than those of three original heat sinks.

References

[1] Jeong, M.W., Jeon,S.W., Kim, Y., Optimal thermal design of a horizontal fin heat sink with a modified-opening model mounted on an LED module, Appl. Therm. Eng., 91 (2015), pp. 105–115.

[2] Cheng, H.H., Huang, D.S., Lin, M.T., Heat dissipation design and analysis of high power LED array using the finite element method, *Microelectron. Reliab.*, 52 (2012), pp. 905–911.

[3] Ahn, B.L., Jang, C.Y., Leigh, S.B., Yoo, S., Jeong, H., Effect of LED lighting on the cooling and heating loads in office buildings, *Appl. Energy*, 113 (2014), pp. 1484–1489.

[4] Ha, M., Graham, S., Development of a thermal resistance model for chip-on-board packaging of high power LED arrays, *Microelectron. Reliab.*, 52 (2012), pp. 836–844.

[5] Shen, Q., Sun, D., Xu, Y., Jin, T., Zhao, X., Orientation effects on natural convection heat dissipation of rectangular fin heat sinks mounted on LEDs, *Int. J. Heat Mass Transfer*, 75 (2014), pp. 462–469.

[6] Christensen, A., Graham, S., Thermal effects in packaging high power light emitting diode arrays, *Appl. Therm. Eng.*, 29 (2009), pp. 364–371.

[7] Elenbaas, W., Heat dissipation of parallel plates by free convection, *Physica*, 9 (1942), pp. 1–28.

[8] Bodoia, J.R., Osterle, J.F., The development of free convection between two heated vertical plates, *J. Heat Transfer*, 84 (1962), pp. 40–44.

[9] Starner, K.E., McManus, H.N., An experimental investigation of free convection heat transfer from rectangular fin arrays, *J. Heat Transfer*, 85 (1963), pp. 273–277.

[10] Welling, J.R., Woolbridge, C.B., Free convection heat transfer coefficients from rectangular vertical fins, *J. Heat Transfer*, 87 (1965), pp. 439–444.

[11] Cha, D.J., Cha S.S., Three-dimensional natural convection flows around two interacting isothermal cubes, *Int. J. Heat Mass Transfer*, 20 (1995), pp. 619–630.

[12] Rao, V.R., Venkateshan, S.P., Experimental study of free convection and radiation in horizontal fin arrays, *Int. J. Heat Mass Transfer*, 39 (1996), pp. 779–789.

[13] Lee, Y.J., Lee, P.S., Chou, S.K., Enhanced thermal transport in microchannel using oblique fins, *J. Heat Transfer*, 134 (2012), p. 101901.

[14] Jones, C.D., Smith, L.F., Optimum arrangement of rectangular fins on horizontal surfaces for free-convection heat transfer, *J. Heat Transfer*, 92 (1970), pp. 6–10.

[15] Bar-Cohen, A., Fin thickness for an optimized natural convection array of rectangular fins, *J. Heat Transfer*, 101 (1979), pp. 564–566.

[16] Bar-Cohen, A., Rohsenow, W.M., Thermally optimum spacing of vertical natural convection cooled parallel plates, *J. Heat Transfer*, 106 (1984), pp. 116–123.

[17] Leung, C.W., Probert, S.D., Shilston, M.J., Heat exchanger design: optimal uniform separation between rectangular fins protruding from a vertical rectangular base, *Appl. Energy*, 19 (1985), pp. 287–299.

[18] Leung, C.W., Probert, S.D., Shilston, M.J., Heat transfer performances of vertical rectangular fins protruding from rectangular bases: effect of fin length, *Appl. Energy*, 22 (1986), pp. 313–318.

[19] Leung, C.W., Probert, S.D., Heat exchanger design: optimal thickness (under natural convective conditions) of vertical rectangular fins protruding upwards from a horizontal rectangular base, *Appl. Energy*, 29 (1988), pp. 299–306.

[20] Leung, C.W., Probert, S.D., Rapley, C.W., Natural convection and radiation from vertically-based arrays of vertical, rectangular fins: a numerical model, *Appl. Energy*, 35 (1990), pp. 253–266.

[21] Vollaro, A.D.L., Grignaffini, S., Gugliermetti, F., Optimum design of vertical rectangular fin arrays, *Int. J. Therm. Sci.*, 38 (1999), pp. 525–529.

[22] Baskaya, S., Sivrioglu, M., Ozek, M., Parametric study of natural convection heat transfer from horizontal rectangular fin arrays, *Int. J. Therm. Sci.*, 39 (2000), pp. 797–805.

[23] Jani, S., Mahmoodi, M., Amini, M., Jam, J. E., Numerical investigation of natural convection heat transfer in a symmetrically cooled square cavity with a thin fin on its bottom wall, *Thermal Science*, 18 (2014), pp. 1119-1132.

[24] Qiu, S., Xu, P., Geng, L., Mujumdar, A. S., Jiang, Z., Yang, J., Enhanced heat transfer characteristics of conjugated air jet impingement on a finned heat sink, *Thermal Science*, 21 (2017), pp. 279-288.

[25] Leung, C.W., Probert, S.D., Heat-exchanger performance: effect of orientation, *Appl. Energy*, 33 (1989), pp. 235–252.

[26] Dayan, A., Kushnir, R., Mittelman, G., Ullmann, A., Laminar free convection underneath a downward facing hot fin array, *Int. J. Heat Mass Transfer*, 47 (2004), pp. 2849–2860.

[27] Mittelman, G., Dayan, A., Dado-Turjeman, K., Ullmann A., Laminar free convection underneath a downward facing inclined hot fin array, *Int. J. Heat Mass Transfer*, 50 (2007), pp. 2582–2589.

[28] Tari, I., Mehrtash, M., Natural convection heat transfer from inclined plate-fin heat sinks, *Int. J. Heat Mass Transfer*, 56 (2013), pp. 574–593.

[29] Jang, D., Yook, S.J., Lee, K.S., Optimum design of a radial heat sink with a fin-height profile for high-power LED lighting applications, *Appl. Energy*, 116 (2014), pp. 260–268.

[30] Jang, D., Yu, S.H., Lee, K.S., Multidisciplinary optimization of a pin-fin radial heat sink for LED lighting applications, *Int. J. Heat Mass Transfer*, 55 (2015), pp. 515–521.

[31] Yu, S.H., Lee, K.S., Yook, S.J., Optimum design of a radial heat sink under natural convection, *Int. J. Heat Mass Transfer*, 54 (2011), pp. 2499–2505.

[32] Huang, G.J., Wong, S.C., Lin, C.P., Enhancement of natural convection heat transfer from horizontal rectangular fin arrays with perforations in fin base, *Int. J. Therm. Sci.*, 84 (2014), pp. 164–174.

[33] Jung, E.D., Lee, Y.L., Development of a heat dissipating LED headlamp with silicone lens to replace halogen bulbs in used cars, *Appl. Therm. Eng.*, 86 (2015), pp. 143–150.

[34] Costa, V.A.F., Lopes, A.M.G., Improved radial heat sink for led lamp cooling, *Appl. Therm. Eng.*, 70 (2014), pp. 131–138.

[35] Wong, K.C., Indran, S., Impingement heat transfer of a plate fin heat sink with fillet profile, *Int. J. Heat Mass Transfer*, 65 (2013), pp. 1–9.

[36] Horikiri, K., Yao, Y., Yao, J., Modelling conjugate flow and heat transfer in a ventilated room for indoor thermal comfort assessment, *Build. Environ.*, 77 (2014), pp. 135–147.

[37] Tari, I., Mehrtash, M., Natural convection heat transfer from horizontal and slightly inclined plate-fin heat sinks, *Appl. Therm. Eng.*, 61 (2013), pp. 728–736.